

# THE EFFECT OF WATER VAPOR AND SUPERALLOY COMPOSITION ON THERMAL BARRIER COATING LIFETIME

B. A. Pint<sup>1</sup>, J. A. Haynes<sup>1</sup>, K. A. Unocic<sup>1</sup> and Y. Zhang<sup>2</sup>

<sup>1</sup>Oak Ridge National Laboratory, Materials Science and Technology Division, Oak Ridge, TN 37831-6156 USA

<sup>2</sup>Tennessee Technological University, Dept. of Mechanical Engineering, Cookeville, TN 38505-0001 USA

Keywords: Thermal barrier coatings, oxidation resistance, water vapor, platinum, MCrAlY, HVOF

## Abstract

New power generation concepts may contain higher water vapor in the turbine combustion gas due to the fuel or to steam dilution. To assess the effect of higher water vapor content on thermal barrier coating performance, furnace cycle (1h) testing was conducted in air with 10, 50 and 90 vol.% water vapor and compared to prior results in dry O<sub>2</sub>. The first series of experiments examined Pt diffusion ( $\gamma+\gamma'$ ) and Pt-modified aluminide ( $\beta$ ) bond coatings on second-generation superalloy N5 at 1150°C with commercially vapor-deposited yttria-stabilized zirconia (YSZ) top coats. Compared to dry O<sub>2</sub>, the average coating lifetimes with Pt diffusion coatings were unaffected by the addition of water vapor while the Pt-modified aluminide coating average lifetime was reduced by >50% with 10% water vapor, but less reduction was observed with higher water contents. A similar set of coatings on low Re superalloy N515 showed no debit in lifetime with Pt aluminide bond coatings exposed to 10% water vapor. Characterization of the alumina scale thickness at failure showed a thicker oxide beneath the YSZ coating (compared to the scale without a top coating) for both types of bond coatings, and an increase in the oxide thickness with the addition of 10% water vapor. These observations were further studied using analytical transmission electron microscopy. The second series of experiments examined high velocity oxygen fuel (HVOF) MCrAlY and MCrAlYHfSi bond coatings and air-plasma sprayed YSZ top coatings on X4 superalloy substrates with and without Y and La additions. Compared to a dry O<sub>2</sub> baseline, the addition of 10% water vapor decreased the YSZ coating lifetime for either bond coating by ~30% at 1100°C. Substrates with Y and La additions showed no change in the average lifetime in 10% water vapor compared to standard X4. A further increase to 50% water vapor did not further decrease the average lifetime of one group of coatings. To better simulate base-load power generation, one group of specimens was cycled with 100h cycles, which substantially increased the coating lifetime. In each case, higher average lifetimes were observed with Hf in the bond coating. Initial characterization of the alumina scales formed at failure showed little effect of the water vapor addition, bond coating composition or substrate composition. For both series of coatings, the addition of 10% water vapor to the experiment reduced YSZ coating lifetime. However, increasing to 50% or 90% H<sub>2</sub>O showed no additional decrease in average YSZ lifetime.

## Introduction

With current concerns about both the environment and the economy, there is a debate about the future of electric power generation in the U.S., where Americans consume ~12MWh/yr/person [1]. As the U.S. recovers from the recent recession, which caused an unprecedented drop in electricity demand, the total annual generation will continue to increase, as

shown in Figure 1. Renewable energy sources are an expensive alternative with significant issues to resolve on durability, deployability (i.e. load matching) and practicality—generating enough electricity using solar photovoltaic cells would require ~180 m<sup>2</sup> of cells/person in the U.S., which is still less than the U.S. crop land devoted to growing corn for ethanol [1]. Fossil fuels will continue to account for most near-term generation. However, over the past decade, the percentage of generation from natural gas has increased by >50% while the role of coal has steadily declined (Figure 1). If abundant, affordable coal is to retain a significant share of future production, clean coal technology will need to be deployed in the coming decade. In fact, two integrated gasification combined cycle (IGCC) plants are under construction (in Indiana and in Mississippi, the latter with 65% carbon capture [2]).

One of the issues to be addressed that will enable wider implementation of IGCC technology is the current de-rating of gas turbines (i.e. firing at a lower maximum temperature) that burn coal-derived synthesis gas (i.e. syngas) due to concerns about component durability [3]. De-rating reduces the turbine efficiency, thus eliminating the de-rating would increase the plant power output and lower the cost of IGCC-generated electricity. In order to develop improved materials/coatings that will reduce or eliminate the de-rating for these turbines, it is critical to understand the reasons for the de-rating. It may be related to improper cleanup (or upset conditions) allowing sulfur or ash into the turbine or the higher water vapor content in the combustion gas [3]. While sulfur or ash contamination could be further mitigated, the exhaust water

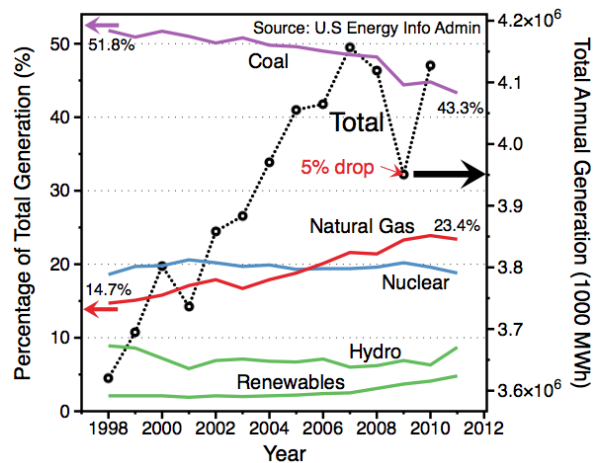


Figure 1. Annual U.S. electricity generation over the past decade and the primary generation sources, showing the decrease in coal usage and increase in natural gas utilization. Data from the U.S. Energy Information Agency.

vapor content is determined by the fuel and combustion conditions. The combustion gas in natural gas- or jet fuel-fired turbines contains ~10 vol.% water vapor. For coal-derived fuels (syngas or hydrogen) or innovative turbine concepts for more efficient carbon capture, the exhaust may contain 30-85% H<sub>2</sub>O due to the combustion reaction residue from gas cleanup or steam dilution to assist with combustion [3-5].

Even though water vapor is present in all combustion turbine hot sections, most laboratory furnace cycling experiments studying thermal barrier coating (TBC) performance are conducted without the addition of water vapor (i.e. laboratory or synthetic air or O<sub>2</sub>). Since Kofstad called water vapor the “forgotten” problem of high temperature oxidation in 1991 [6], there has been a steadily building interest in the role of water vapor [7-18]. Even though alumina-forming alloys and coatings (including TBC bond coatings) are thought to be more resistant to water vapor than chromia-forming alloys, they are still affected by its presence. The need to clarify the role of water vapor content on TBC performance is now apparent; any detrimental effect needs to be better understood and mitigated. This on-going study began by first building on prior results: (1) average YSZ lifetime with two phase ( $\gamma+\gamma'$ ) Pt diffusion [19-23] and Pt-modified ( $\beta$ -NiPtAl) aluminide bond coatings in furnace cycling at 1150°C in dry O<sub>2</sub> [24] and (2) alumina scale formation at 1100°C in air with 10-90% water vapor on similar Pt-containing bond coatings and model alloys (but without YSZ top coats) [12,23]. Without the YSZ coating, the prior results were similar to other work suggesting increased alumina scale spallation and more transient oxide formation with increasing water vapor content [9,10]. The current study also examined MCrAlY bond coating more relevant to large land-based turbines [25,26]. In both types of TBC, the addition of 10% water vapor decreased average coating (YSZ) lifetime, except Pt diffusion ( $\gamma+\gamma'$ ) coatings, which were unaffected. However, higher water vapor contents did not further reduce YSZ lifetime, suggesting that the source of IGCC turbine de-rating is not the higher water vapor contents in the exhaust gas.

### Experimental Procedure

For fabricating the Pt-containing coatings, coupons of second generation single crystal superalloys René N5 and low Re N515 [27] (Table 1) 1.5mm thick, ~16mm diameter and chamfered edges were grit blasted with alumina and then electroplated with 7±1 µm of Pt in a laboratory scale bath at Tennessee Technological University. For the Pt diffusion coatings, the plated coupons were then annealed in a vacuum of 10<sup>-4</sup>Pa (10<sup>-6</sup>Torr) for 2h at 1175°C resulting in a ~25µm thick coating [22]. For Pt-modified aluminide coatings, the plated specimens were aluminized for 6h at 1100°C to form a ~40µm thick  $\beta$  layer in a laboratory-scale chemical vapor deposition reactor, described elsewhere [28]. A ~125µm thick YSZ top coat was deposited on one side of the coupons by electron-beam physical vapor deposition (EB-PVD)

using a standard commercial process that included a light grit blasting prior to YSZ deposition. For the MCrAlY and MCrAlYHfSi bond coatings, coupons of three variants of CMSX-4 (Table 1) 2mm thick, ~16mm diameter and chamfered edges were high velocity oxygen fuel (HVOF) coated using a commercial-type process and commercial NiCoCrAlY and NiCoCrAlYHfSi [29,30] powders at Stonybrook University. The HVOF-coated specimens were annealed in a vacuum of 10<sup>-4</sup>Pa for 4h at 1080°C and had a bond coating thickness of ~150µm. Coupons were then returned to Stonybrook University for air-plasma spraying (APS) a 125µm-thick YSZ layer on one side using standard conditions.

Groups of four specimens were evaluated at each condition: three were coated with YSZ and the fourth was tested without YSZ (and without grit blasting for both diffusion coatings) to study the alumina scale surface morphology evolution. The specimens were hung by a Pt-Rh wire in an automated cyclic rig and exposed for 1h at 1100°C (MCrAlY) or 1150°C (Pt-containing) in dry O<sub>2</sub> or air with 10±1%, 50±2% or 90±2% vol.% water vapor and cooled in laboratory air for 10min for each cycle. One set of specimens was held in an alumina boat and cycled in 100h cycles in an alumina tube furnace in air with 10% H<sub>2</sub>O, where the specimens were slowly heated to temperature to prevent cracking of the furnace ware. Oxidation in wet air was conducted by flowing air at 850 ml/min with distilled water atomized into the gas stream above its condensation temperature. The injected water was measured to calibrate its concentration [12]. A Mettler-Toledo model AG245 balance was used to measure mass change every 20 cycles. Every 200 cycles, the specimens without YSZ were characterized by scanning electron microscopy (SEM) equipped with an energy dispersive x-ray spectrometer (EDS) to examine the surface scale adhesion and by profilometry (six 1cm laser line scans or 5, ~1x1mm areas on a Veeco Wyko model NT9100 optical profilometer) to measure roughness. After completing testing, the specimens were metallographically sectioned and examined by light microscopy and SEM. In some cases, specimens were Cu-coated before sectioning to protect the scale. Transmission electron microscopy samples were prepared via the focused ion beam (FIB) in-situ lift-out technique using a Hitachi NB5000 FIB-SEM. During FIB specimen preparation, a W/C layer was deposited to protect the gas interface of the scale. TEM specimens were characterized by electron diffraction and EDS analysis using a Philips model CM200 scanning-transmission electron microscope (STEM) equipped with a Schottky field emission gun (FEG) operated at 200kV.

### Results

#### Pt-containing Diffusion/EB-PVD Coatings at 1150°C

Figure 2 summarizes the average lifetime data for the Pt-containing bond coatings on N5 and N515 including the dry O<sub>2</sub> and 10% and 90% H<sub>2</sub>O results for N5 reported previously

Table 1. Chemical compositions (atomic% or ppma) determined by inductively coupled plasma analysis and combustion analysis.

Material	Ni	Cr	Al	Re	Co	W	Ta	Mo	Ti	Other (ppma)
N5	64.7	8.0	13.3	0.9	7.6	1.6	2.2	0.9	0.01	132Zr,70Y,540Hf,17S
N515	66.5	6.6	13.2	0.5	7.3	2.0	2.1	1.2	<0.002	66Zr,104Y,1993Hf,13Ce,<1S
X4	62.8	7.5	13.0	0.9	9.7	2.1	2.2	0.4	1.2	<3Y,270Hf,17S
X4-1	62.9	7.3	12.8	0.9	9.8	2.1	2.2	0.4	1.2	1-2Y,2-3La,340Hf,<1S
X4-2	63.1	7.3	12.8	0.9	9.8	2.1	2.2	0.4	1.2	10-14Y,6-9La,270Hf,<1S
MCrAlYHf	41.2	16.2	22.9		18.4					3860Y,710Hf,6500Si,3S

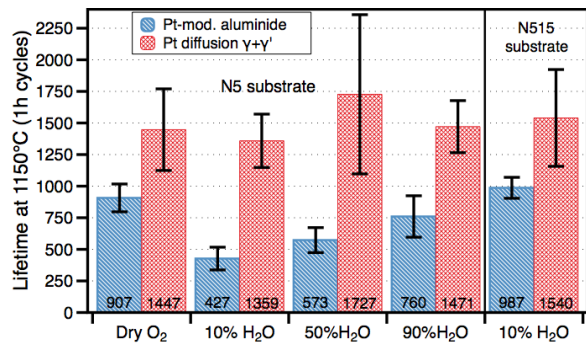


Figure 2. Average lifetimes for EB-PVD YSZ-coated N5 and N515 specimens exposed in 1h cycles at 1150°C in several environments. The bars note the standard deviation for 3 specimens of each type.

[24,31,32]. The lifetime was defined as loss of 20% of the YSZ top coat but most specimens showed massive spall at failure. The bars for each set show the standard deviation of the three specimens. Mass change data are not reported because mass losses were typical dominated by edge spallation of the YSZ. For the dry O<sub>2</sub> results, the averages are higher than other studies [33-35] but direct comparisons with other studies are difficult because of differences in coating fabrication, specimen geometry and thermal cycling. The results for Pt diffusion ( $\gamma+\gamma'$ ) coatings in Figure 2 indicate that the addition of water vapor had little effect on the average lifetime but considerable scatter was observed. In contrast, the average lifetime of the Pt-modified aluminide ( $\beta$ ) coatings on N5 was significantly reduced, especially by 10% H<sub>2</sub>O. For the N5 substrates, the reduction in average lifetime was inversely proportional to the water content, a 53% reduction with 10% H<sub>2</sub>O, 37% with 50% H<sub>2</sub>O and 16% with 90% H<sub>2</sub>O (the 90% H<sub>2</sub>O life is within a standard deviation of the dry O<sub>2</sub> lifetime). For the  $\beta$  coating on N515 substrates, the average in 10% H<sub>2</sub>O was more than double that observed for N5 and slightly higher than for N5 substrates in dry O<sub>2</sub>, Figure 2. No comparable dry O<sub>2</sub> data has been generated for coated N515 substrates.

Figure 3 shows the change in the root mean square (RMS) roughness (Rq) with exposure time for the coated specimens without a YSZ coating. It was confirmed previously that similar values were obtained for the optical and laser profilometry measurements [31]. All of the Pt diffusion coatings on N5 showed very similar roughness and very little change with exposure time to 1500h. The measured roughness of the Pt diffusion coating on N515 was slightly higher. In contrast, the rate of roughening or “rumpling” [36,37] for the Pt-modified aluminide coatings was much faster in the wet air environments compared to dry O<sub>2</sub>. The fastest rumpling rate was observed on the specimen exposed to 10% H<sub>2</sub>O which correlates to the shortest average coating lifetime, Figure 2. The time to a Rq value of ~5 seems to be a fair prediction of the average lifetime. However, these roughness measurements are from the specimen without a YSZ top coat. The amount of rumpling was greatly reduced with the presence of the YSZ layer as shown in Figure 4 and attributed to the constraint of the adjacent ceramic layer [38-40].

Figures 4-6 show cross-sections of representative failed specimens comparing dry O<sub>2</sub> and air with 10% or 50% H<sub>2</sub>O. The sections are from failed YSZ-coated specimens so they do not all have the same

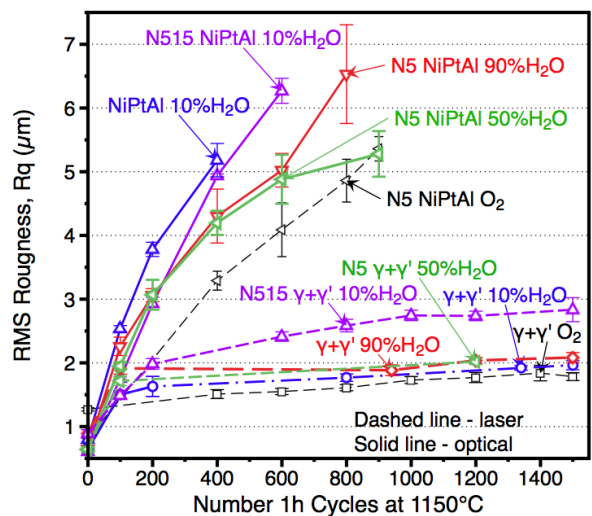


Figure 3. Root mean square (RMS) roughness (Rq) for the coated N5 and N515 specimens without a YSZ coating as a function of 1h cycles at 1150°C. Dashed lines show laser profilometry and solid lines are from an optical profilometer.

exposure times. The top half of each image shows the bond coating beneath the YSZ layer and the bottom half shows the coating on the opposite side of the specimens without the YSZ layer. For the Pt-modified aluminide bond coatings in Figure 4, clearly the roughness (i.e. rumpling) was higher on the bottom side where the coating was not constrained by the YSZ top coat, as was also noted in the prior dry O<sub>2</sub> study [24]. The difference between the two sides could be attributed to the light grit blasting on one side prior to YSZ deposition, however, roughening the surface has been found to *increase* deformation [41]. The cross-sections in Figure 4 only provide a qualitative comparison of a single region. However, the specimen exposed to 10% H<sub>2</sub>O (Figure 4b) shows similar rumpling (without YSZ) after only 420 1-h cycles as the specimen exposed for 800h in dry O<sub>2</sub> (Figure 4a). This is consistent with the roughness data in Figure 3. In the light microscopy images, the  $\beta$  (slightly darker gray) and  $\gamma'$  phases are discernable and are labeled in Figure 4. As expected, more  $\beta$  is retained for the shorter exposure time in 10% H<sub>2</sub>O. As interdiffusion occurs during exposure, the high Al content  $\beta$  phase transforms to the lower Al content  $\gamma'$  phase. Rumpling of the Pt-modified aluminide bond coating could be attributed to interdiffusion [37] or the  $\beta+\gamma'$  to  $\beta$  phase transformation (which occurs during each thermal cycle) [42]. However, neither hypothesis appears to explain the increased roughening in the presence of water vapor. Nevertheless, the increased roughening can explain the decrease in coating life observed, especially in air with 10% H<sub>2</sub>O. Rumpling causes cracks to propagate at the YSZ-bond coating interface, Figure 4.

The lower portion of Figure 5 is shown at the same magnification as Figure 4 in order to emphasize that the Pt diffusion bond coatings remained essentially flat during much longer exposures, 1740 and 2060 cycles in dry O<sub>2</sub> and air with 50% H<sub>2</sub>O, respectively. This is also consistent with the roughness data in Figure 3. The upper portion of Figure 5 is shown at a higher magnification in order to better observe the interface region and the alumina scale. For the  $\gamma+\gamma'$  coatings, failure occurred primarily

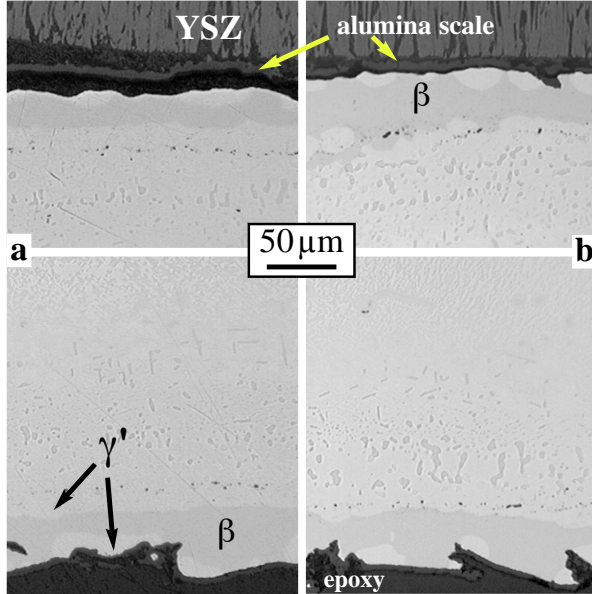


Figure 4. Light microscopy of polished sections of YSZ-coated N5 specimens with Pt-modified aluminide bond coatings after YSZ coating failure at 1150°C after (a) 800 1-h cycles in O<sub>2</sub> and (b) 420 1-h cycles in 10% H<sub>2</sub>O. Images show the coating beneath the YSZ at the top and the coating on the opposite side of the specimen without a YSZ overlayer at the bottom.

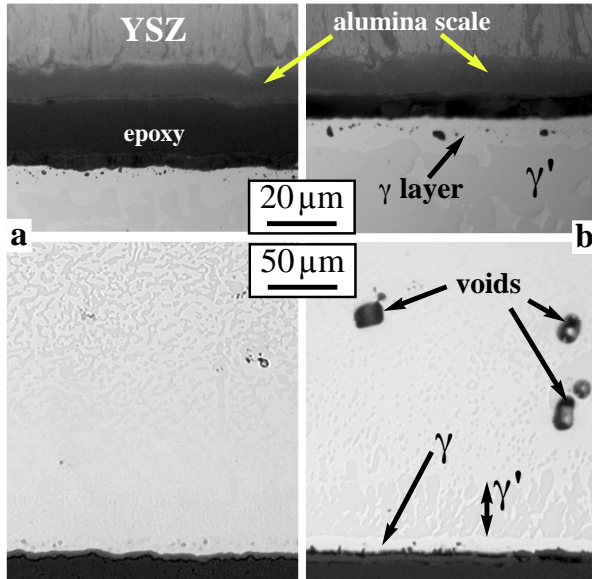


Figure 5. Light microscopy of polished sections of YSZ-coated N5 specimens with Pt diffusion bond coatings after YSZ coating failure at 1150°C after (a) 1740 1-h cycles in O<sub>2</sub> and (b) 2060 1-h cycles in 50% H<sub>2</sub>O. Images show the coating beneath the YSZ at the top and the coating on the opposite side of the specimen without a YSZ overlayer at the bottom.

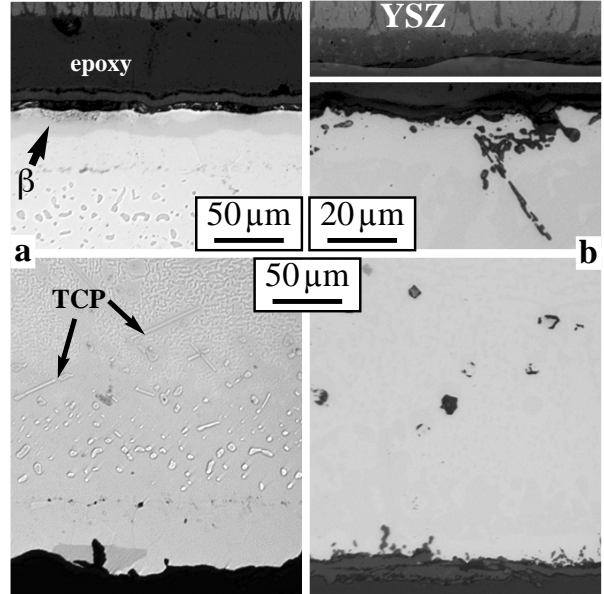


Figure 6. Light microscopy of polished sections of YSZ-coated N515 specimens cycled to coating failure in air with 10% H<sub>2</sub>O at 1150°C (a) Pt-modified aluminide bond coating after 920 1-h cycles and (b) Pt diffusion coating after 1720 cycles. Images show the coating beneath the YSZ at the top and the coating on the opposite side of the specimen without a YSZ overlayer at the bottom. Topologically close-packed (TCP) phases shown in (a).

at the metal-alumina interface with the scale attached to the YSZ top coat. The metal adjacent to the alumina appears to be a complete  $\gamma$  (Ni solid solution) layer and the nearly continuous  $\gamma'$  layer appears to extend  $\sim 40\mu\text{m}$  into the substrate after 2060h at 1150°C, Figure 5b. Similar structures have been identified by electron microprobe analysis (EPMA) in previous studies [22-24]. Kirkendall voids also are observed in all the Pt diffusion coatings.

Figure 6 shows images from the coatings on N515 at similar magnifications as Figures 4 and 5. One obvious difference seen in Figure 6b is the increased internal oxidation (oxide stringers penetrating into the substrate). This is attributed to the higher Hf in N515 compared to N5, Table 1. Previous studies of  $\gamma+\gamma'$  coatings on high Hf directionally solidified alloys showed similar accelerated oxidation [23]. Differences in the coating interdiffusion zones between N5 and N515 including the composition of refractory-rich precipitates (e.g., Figure 6a) are currently being characterized.

Each of the failed sample cross-sections from each group was examined by SEM and 40 scale thickness measurements were made on each specimen. That data set is summarized in Figure 7 as a function of the square root of exposure time, assuming a parabolic relationship. The  $\beta$  and  $\gamma+\gamma'$  coatings are both included with the former on the left (shorter lifetimes) and the latter on the right (longer lifetimes) with the data for each substrate and condition fit to one line. Figure 7a shows the data points (and standard deviations) from N5 in dry O<sub>2</sub> and 10% H<sub>2</sub>O and N515 (10% H<sub>2</sub>O). For all these conditions, the scale formed beneath the YSZ coating was thicker than the opposite side without a YSZ top

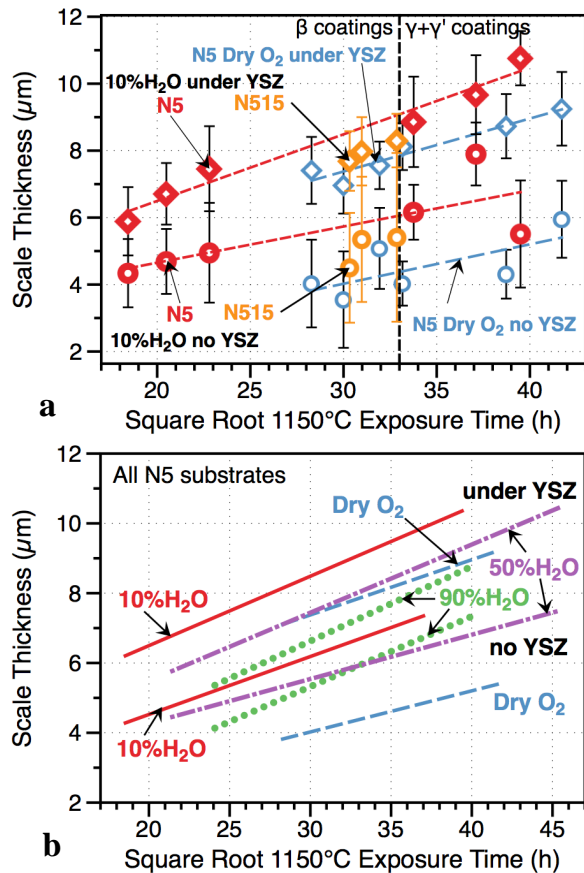


Figure 7. Average alumina scale thickness as a function of the square root of exposure time (1h cycles to failure) at 1150°C for the specimens with Pt-containing bond coatings and YSZ on one side. The thickness with and without the YSZ layer in two environments is shown (a) data with standard deviation (bars) for N5 in dry  $\text{O}_2$  and N5 and N515 in 10%  $\text{H}_2\text{O}$ ; (b) summary of N5 data in all four environments.

coat. Spallation (from the uncoated side) could explain some of this difference but there was little indication of spallation in plan view. More importantly, there appeared to be a thicker oxide formed in the presence of water vapor than in dry  $\text{O}_2$ . A thicker scale with a higher strain energy due to the thermal expansion mismatch with the substrate [43] could explain the early failure for the  $\beta$  coatings but did not appear to affect the YSZ lifetime of the Pt diffusion bond coatings. The scale formed on N515 substrates was slightly thinner than that formed on N5, although not a significant difference given the scatter seen in Figure 7a. This difference could be attributed to the higher Hf content in N515 having a beneficial effect on the scale growth [44-46]. Given the large number of data points, Figure 7b shows just the fitted lines for each N5 condition on both sides of the specimen (with and without YSZ). The general trend is that higher water vapor contents (50 and 90%) did not show as strong of an effect on the scale thickness as 10%  $\text{H}_2\text{O}$ . Under the YSZ top coat, the scale was similar in thickness to dry  $\text{O}_2$ . Without the YSZ top coat, the scale thicknesses at 50 and 90%  $\text{H}_2\text{O}$  were higher compared to dry  $\text{O}_2$ .

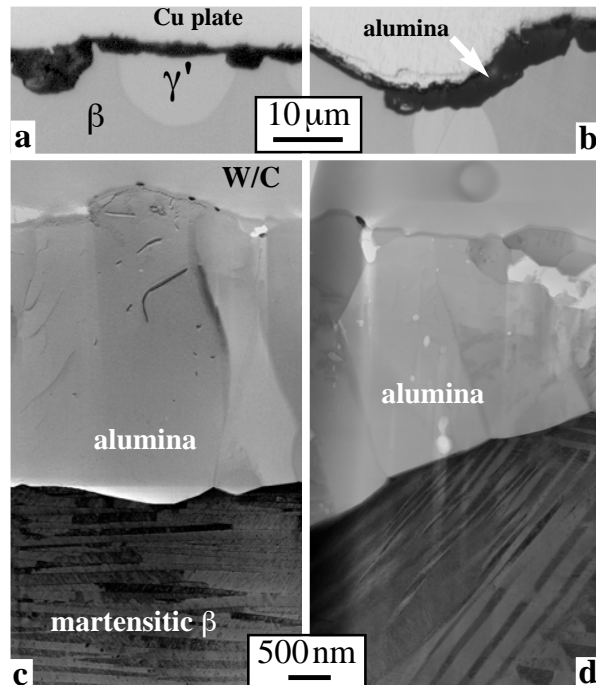


Figure 8. Light microscopy (a,b) and STEM bright field images (c,d) of the alumina scale formed on Pt aluminide bond coatings on N5 without a YSZ top coating after 900 1-h cycles at 1150°C in (a,c) dry  $\text{O}_2$  and (b,d) air with 50%  $\text{H}_2\text{O}$ .

To learn more about the scale being formed in the different environments, TEM cross-sections of the scale formed on the specimens without a YSZ top coat were examined. This makes specimen preparation easier and standardizes the exposure time. Figure 8 shows both light microscopy and TEM cross-sections of the scale formed on  $\beta$  coatings on N5 oxidized in dry  $\text{O}_2$  and air with 50%  $\text{H}_2\text{O}$ . As was observed by TEM at 1100°C on cast NiAl+Hf [24], there is not a major effect of water vapor on the scale microstructure. The variation in oxide thickness observed in the TEM sections (Figures 8c and 8d) must be considered in light of the variable scale thickness observed at lower magnification (Figures 8a and 8b). There is no striking difference in grain structure or defect density. In general, the scale looks like what is expected to form on a Pt-modified  $\beta$ -phase coating [44,45,47]. Initial analysis of the scale grain boundaries found Hf segregation in both specimens. In both cases, the underlying substrate clearly shows the expected martensitic  $\beta$  structure after 900h at 1150°C [42,48,49].

Figure 9 shows a comparison of the scales formed on Pt diffusion coatings on N5 after 1500h in dry  $\text{O}_2$  and air with 10%  $\text{H}_2\text{O}$ . For these  $\gamma+\gamma'$  coatings, the scales are more uniform in thickness (Figure 5) and the difference in scale thickness in the TEM section is more representative of the overall specimen. While the scale formed in the presence of water vapor was thicker, the grain structure was similar, with finer columns than was observed on the  $\beta$  coatings (Figure 8), which is consistent with previous observations [47]. In both cases, the smaller grains at the gas interface are spinel type oxides rich in Ni and Cr, while the underlying grains are  $\alpha\text{-Al}_2\text{O}_3$ . Near the spinel-alumina interface,

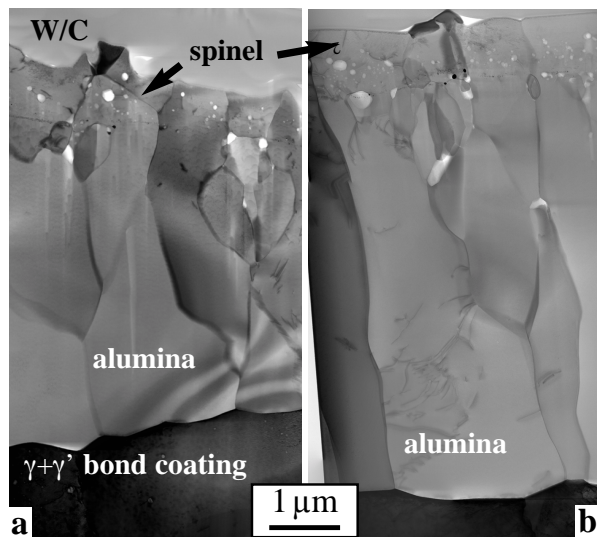


Figure 9. STEM bright field images of the alumina scale formed on Pt diffusion bond coatings on N5 without a YSZ top coating after 1500 1-h cycles at 1150°C in (a) dry O<sub>2</sub> and (b) air with 10% H<sub>2</sub>O.

there are numerous pores, which also has been observed in other systems [47,50,51]. Figure 10 shows the scale formed on N515 with a Pt diffusion coating after 1500h in air with 10% H<sub>2</sub>O. The scale structure is very similar to that formed on N5. The section captured one of the smaller oxide stringers evident in Figure 6b. Two EDS maps are shown in Figures 10b and 10c from the boxes indicated in Figure 10a. Near the gas interface, the Ni map clearly shows the spinel layer that also was observed in the specimens in Figure 9. In the metal near the gas interface, the oxide stringer

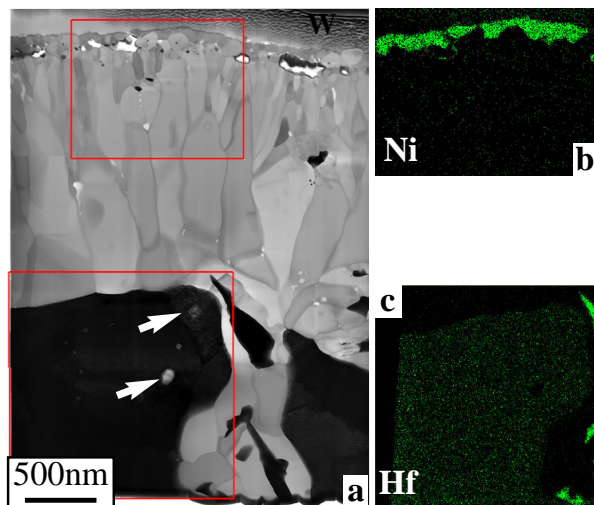


Figure 10. (a) STEM bright field image of the alumina scale formed on N515 with a Pt diffusion coating oxidized for 1500h at 1150°C in 10% H<sub>2</sub>O. (b) Ni x-ray map from upper box in (a); (c) Hf x-ray map from lower box in (a).

penetrating into the substrate contains Hf-rich precipitates but the oxide particles in the metal (arrows in Figure 10a) are not Hf-rich. Additional analytical TEM results will be published as these specimens and others from this group are further analyzed.

#### HVOF/APS Coatings at 1100°C

While diffusion coatings are used in aero-type engines, these turbines are not likely to use syngas or hydrogen fuels. Large, land-based power generation turbines typically use sprayed MCrAlY-type bond coatings and sprayed YSZ top coatings [25,26]. A second series of experiments was conducted using HVOF-sprayed MCrAlY-type coatings and APS YSZ top coatings. Figure 11 summarizes the results for this series where variants of a different superalloy (X4) were used. In this case, the oxidation temperature was reduced to 1100°C. The higher thermal expansion of MCrAlY compared to  $\beta$  or  $\gamma$ - $\gamma'$  restricts the maximum use temperature for these coatings. The higher mismatch between the substrate and the alumina scale means that scale spallation will occur at a lower critical scale thickness due to the increased strain energy in the scale after cooling from temperature [43,54]. In this series, a strategy for improving was TBC lifetime was explored by using variations of X4 with Y and La additions (alloys designated X4-1 and X4-2, Table 1). Also, two different bond coatings with similar compositions were used to explore the benefit of Hf and Si additions to the bond coating [29]. As expected, the Hf-containing bond coating showed a higher lifetime than the base MCrAlY coating in each case. However, for the base X4 substrate, the time to failure for both bond coatings was reduced by ~30% when the cycling was conducted in air with 10% H<sub>2</sub>O. Except for the MCrAlYHfSi coatings in dry O<sub>2</sub>, the scatter in the lifetimes with the X4 substrate was relatively low. The effect of Y and La doping of X4 was explored by comparing the performance of one set of coatings with each substrate in air with 10% H<sub>2</sub>O. Figure 11 shows very little difference in the lifetimes of either bond coating among the three substrates in the wet air environment. Finally, one set of X4-2 substrates was cycled in air with 50% H<sub>2</sub>O. Similar to the result for the diffusion coatings, increasing the water vapor content did not further decrease the coating lifetime (Figure 11). The last group of coatings on the X4-1 substrate were cycled at 1100°C in air with 10% water vapor but the cycle frequency was increased to

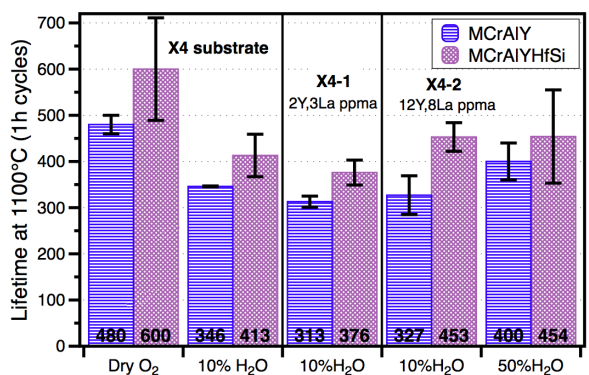


Figure 11. Average lifetimes for APS YSZ-coated X4 specimens (with and without Y/La additions) with two different HVOF MCrAlY-type bond coatings exposed in 1-h cycles at 1100°C in three environments. The bars note the standard deviation for 3 specimens of each type.

100h, which is more comparable to base load power generation than 1h cycles. Compared to the lifetimes observed in 1h cycles, Figure 12 shows that the change to 100h cycles had a dramatic effect on the coating lifetime, especially for the bond coating containing Hf where only one of the coatings has failed after 30 cycles (3,000h) and two coatings have not reached failure after 35 cycles. A very large standard deviation was observed for the three MCrAlY bond coatings because two failed after 300h (comparable to the 1h cycle life) but the third one retained its YSZ layer for 22 cycles (2200h) until a delamination was determined to have exceeded the 20% failure criteria.

Figure 13 shows representative cross-sections of the two bond coatings on standard X4 after failure in dry O<sub>2</sub> and air with 10% H<sub>2</sub>O. In both conditions and for both bond coatings, the majority of the YSZ coating spalled at failure with only small bits remaining attached (Figures 13c-13f). At lower magnification (Figures 13a and 13b), the bond coatings all show an outer layer depleted in the Al-rich  $\beta$  phase and a  $\gamma'$  layer at the coating-substrate interface due to interdiffusion with the X4 substrate. Remnants of the surface grit blasting remain at the original substrate interface. There are only minimal differences between the two coatings and two environments. At higher magnification (Figures 13c-13f), the remaining scale typically could be observed in select locations where the bond coating was locally rougher. As with the Pt containing bond coatings, it is difficult to draw conclusions about the effect of Hf or H<sub>2</sub>O on the scale thickness because of the different failure times. However, Figure 14 shows initial results to measure the scale thickness on a few representative specimens. As is apparent in Figure 13, the scale thickness is variable. In this case, there does not appear to be much difference in oxide thickness between the side coated with YSZ and the opposite side without YSZ. Also, the addition of Hf did not appear to change the oxide thickness in dry O<sub>2</sub>, Figure 14. The specimens exposed to 10% H<sub>2</sub>O failed at shorter times than those exposed in dry O<sub>2</sub>. Thus, there appears to be a slight increase in the oxide thickness in the presence of water vapor. However, more measurements are needed to verify this trend such that plots like Figure 7 can be generated.

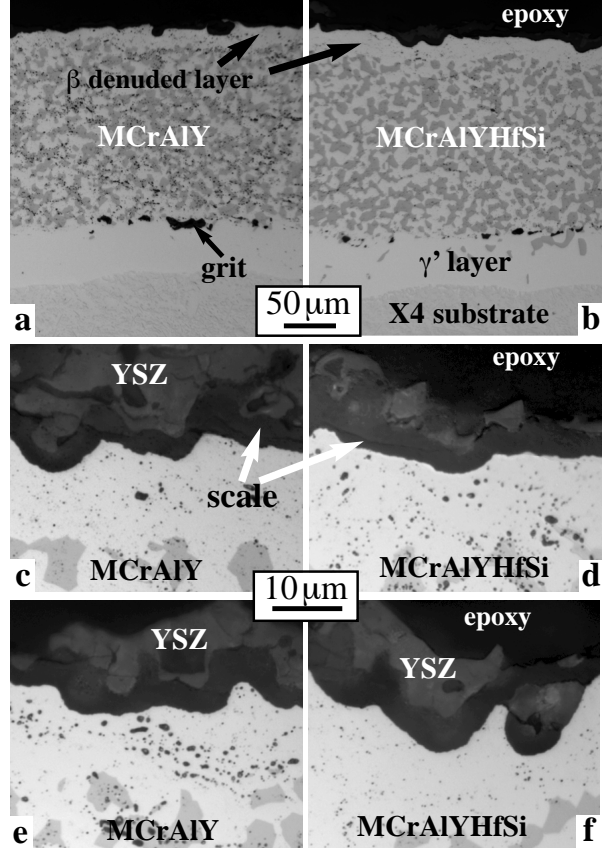


Figure 13. Light microscopy of polished sections of APS YSZ-coated X4 specimens with two MCrAlY bond coatings after YSZ coating failure at 1100°C after (a,e) 346 1-h cycles in 10% H<sub>2</sub>O; (b,f) 360 1-h cycles in 10% H<sub>2</sub>O; (c) 460 1-h cycles in O<sub>2</sub> and (d) 580 1-h cycles in O<sub>2</sub>;

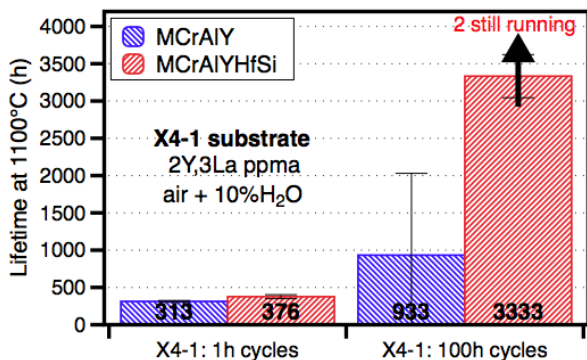


Figure 12. Average lifetimes for APS YSZ-coated X4-1 specimens doped with 2Y and 3La (ppma) with HVOF MCrAlY-type bond coatings exposed in 10% water vapor in 1h and 100h cycles. The bars note the standard deviation for 3 specimens of each type.

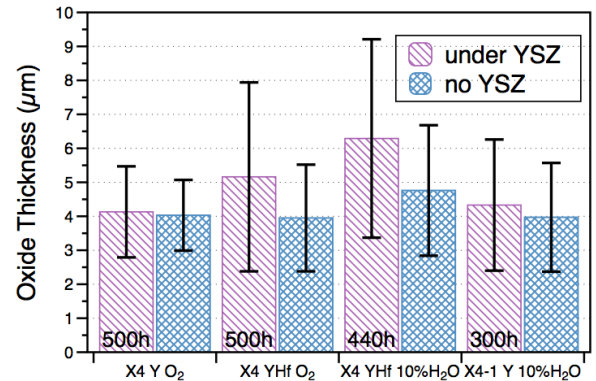


Figure 14. Average alumina scale thickness for several different conditions (designated: superalloy, bond coating, environment). A large scatter (bars show standard deviation) was detected in each condition after coating failure at 1100°C in 1h cycles.

## Discussion

The working hypothesis when beginning this study was that there was significant evidence [9,10,16] that the addition of water vapor would have a negative effect on coating lifetime and presumably higher concentrations would be worse. The addition of water vapor did prove to have a detrimental effect on coating lifetime in most cases. However, there was no indication from these furnace cycle tests that 50% or 90% water vapor were more detrimental to coating lifetime than 10% H<sub>2</sub>O, which is nominally what is present in turbines burning natural gas and jet fuel. Also, the previous hypothesis that the low Al content  $\gamma+\gamma'$  bond coatings would form more Ni-rich oxide and be adversely affected by water vapor [12,23] was disproven. The Pt diffusion coatings were the only bond coating that was virtually immune from water vapor in these experiments (Figure 2). The Ni-rich oxide on the coatings (Figure 10) was considerably less than observed on model  $\gamma+\gamma'$  NiPtAl cast alloys [23], perhaps due to a finer alloy grain size in the coatings. The Ni-rich spinel-alumina interface tends to be weak with numerous voids, likely due to the solid state reaction between alumina and NiO to form spinel [56]. However, Ni-rich oxide was difficult to locate at the YSZ-alumina interface by SEM and only ~100nm thick on the scale formed on the  $\gamma+\gamma'$  coating without YSZ.

It was surprising that 10% H<sub>2</sub>O produced the largest drop in aluminide coating lifetime. In cyclic testing of cast NiAl+Hf and NiCrAlYHf alloys at 1100°C [12,23], an increasing reduction in mass gain was observed for increasing additions of water vapor from 10-90%. This mass difference could be a change in the scale growth rate or could be caused by minor spallation or evaporation. The mass change data for the diffusion coated specimens at 1150°C was difficult to interpret and did not change monotonically with water content. The increased roughness observed with the addition of water vapor for the aluminide bond coatings is consistent with the decrease in lifetime observed, especially for 10% H<sub>2</sub>O. (Consistent with other studies [37], no increase in roughness was observed at 1100°C [23].) However, a mechanistic explanation for the increased rate of roughening has not been identified. This observation does not appear to match any of the current mechanisms for rumpling or water vapor effects. Early stage studies of the stress in the alumina scale are underway to determine if water vapor affects residual stress in the alumina scale. One issue to consider is that, with air as the carrier gas, the O<sub>2</sub> content was varied as well as the H<sub>2</sub>O content in these experiments and no nitrogen was present in the dry O<sub>2</sub> experiment. Perhaps evaluating additional environments would lead to a better understanding.

The previous water vapor study at 1100°C also found evidence for evaporation of Al(OH)<sub>3</sub> at 1100°C [12]. With a YSZ overlayer, evaporation should be limited in a TBC system. That could explain the thicker oxide formed under the YSZ in wet air, Figure 7, but does not explain the difference in dry O<sub>2</sub>. Water vapor also could affect the transport through the alumina scale. Recent work studying the isothermal alumina scale growth rate in the presence of water vapor has shown that water vapor *reduces* the scale thickness at 1100°-1200°C [57,58]. However, these studies were conducted on FeCrAl-type alloys that do not form base-metal oxide layers like NiCrAl or NiPtAl compositions. The hypothesis that the slower growth in Ar-H<sub>2</sub>-H<sub>2</sub>O compared to Ar-O<sub>2</sub> was due to the lower oxygen partial pressure [57] was disproven when a similar decrease was observed when comparing dry O<sub>2</sub> and Ar or air with 10% H<sub>2</sub>O [58]. A different diffusing species, such as an OH<sup>-</sup> ion, could explain the change in rate but it is not clear why the

OH<sup>-</sup> species would be preferred over a faster diffusing O<sup>2-</sup> ion in wet air. Furthermore, there was no indication in the current work that water vapor reduced the scale growth rate.

The results on low Re N515 appear to be more affected by the higher Hf in this alloy than the other composition changes, Table 1. Figure 6a shows some of the precipitates in the alloy formed due to coating interdiffusion. Comparison with N5 may reveal more about the coating compatibility of this alloy. The higher Hf content does not appear compatible with the  $\gamma+\gamma'$  bond coating based on the increased internal oxidation. However, coating lifetime was not reduced (Figure 2). Higher Hf may be beneficial with aluminide coatings as suggested by the >2X higher lifetime in air with 10% H<sub>2</sub>O compared to N5.

For the HVOF coating results, the Y and La doped X4 superalloys did not appear to improve TBC lifetime in this study, Figure 11. Previous work with the MCrAlYHfSi bond coating without a YSZ top coat was not able to measure any difference in alumina growth rate or adhesion with the doped superalloys [59]. Characterization found no indication of La diffusing through the bond coating into the alumina scale. However, there was evidence for Ti from the superalloy diffusing through the bond coating [60]. The Hf-containing bond coating does appear to be a promising strategy, one that was developed nearly 30 years ago [29].

One issue with the HVOF coating specimens is that the roughness (Ra ~5-6 $\mu$ m) is not as high as commercial coatings in turbines (~10 $\mu$ m). This was a first batch of specimens fabricated and will need to be evaluated in subsequent experiments. As a final note, the temperatures were selected for this study to induce failure in a reasonable amount of time. These temperatures are much higher than the typical (~900°C) metal temperatures in land-based gas turbines where the required TBC lifetime is >25 kh. This raises the issue that water vapor may have a different effect in this temperature range. Further work is needed to understand water vapor effects over a range of conditions.

## Summary

Furnace cycling at 1100° and 1150°C was used to compare the YSZ coating lifetime in two different types of TBC systems with and without the presence of water vapor. At 1100°C, MCrAlY-type bond coatings and APS YSZ top coatings on X4 substrates showed a ~30% reduction in average TBC lifetime in air with 10% H<sub>2</sub>O compared to dry O<sub>2</sub> for both MCrAlY and MCrAlYHfSi bond coatings. The latter coatings showed a longer YSZ lifetime in both environments. Superalloys with Y and La additions showed no effect on the coating lifetime in air with 10% H<sub>2</sub>O and increasing the water vapor to 50% did not further decrease the lifetime. At 1150°C, the average EB-PVD YSZ lifetime with Pt-diffusion bond coatings on N5 superalloy substrates was similar in dry O<sub>2</sub> and air with 10%, 50% or 90% water vapor. In contrast, the addition of 10% water vapor resulted in a >50% lifetime reduction for Pt-modified aluminide bond coatings compared to dry O<sub>2</sub> at 1150°C. With 50% water vapor, the average TBC lifetime dropped by 37% but only 16% with 90% H<sub>2</sub>O, which was not statistically different than in dry O<sub>2</sub>. The decrease in lifetime can be attributed to more rapid surface roughening of the Pt-modified aluminide coating in the presence of water vapor, which led to more rapid coating failure. However, a mechanism for this observed change in roughening has not been identified. There is no evidence from this study that increased (>10-15%) levels of water vapor in IGCC turbines would degrade coating performance. Nevertheless, most

TBCs are exposed to water vapor in service, thus, testing in water vapor appears necessary to develop coatings resistant to the detrimental effect of water vapor.

### Acknowledgements

The authors would like to thank Ben Nagaraj at General Electric and Ken Murphy at Howmet for their assistance. At ORNL, the authors are grateful to the technical support of G. Garner, H. Longmire, L. Walker, T. Lowe, K. M. Cooley and D. W. Coffey. This research was sponsored by the U.S. Department of Energy, Office of Coal and Power R&D, Office of Fossil Energy, (R. Dennis program manager) and the Assistant Secretary for Energy Efficiency and Renewable Energy, Industrial Technologies Program (Combined Heat and Power).

### References

1. P. Denholm and R. M. Margolis, "Land-use requirements and the per-capita solar footprint for photovoltaic generation in the United States," *Energy Policy*, 36 (2008), 3531-3543.
2. [www.mississippipower.com/kemper/Facts.asp](http://www.mississippipower.com/kemper/Facts.asp)
3. I. G. Wright and T. B. Gibbons, "Recent developments in gas turbine materials and technology and their implications for syngas firing," *International Journal of Hydrogen Energy*, 32 (2007), 3610-3621.
4. P. Chiesa, G. Lozza and L. Mazzocchi, "Using Hydrogen as Gas Turbine Fuel," *Journal of Engineering for Gas Turbines & Power*, 127 (2005), 73-80.
5. L. A. Ruth, "Advanced clean coal technology in the USA," *Materials at High Temperature*, 20 (2003), 7-14.
6. P. Kofstad, "High Temperature Corrosion of Metals," *Microscopy of Oxidation I*, ed. M. J. Bennett and G. W. Lorimer (London, UK: Institute of Metals, 1991), 2-9.
7. C. Leyens, K. Fritscher, R. Gehrting, M. Peters and W. A. Kaysser, "Oxide Scale Formation on an MCrAlY Coating in Various H<sub>2</sub>-H<sub>2</sub>O Atmospheres," *Surface and Coatings Technology*, 82 (1996), 133-144.
8. B. Jönsson B, C Svedberg, "Limiting Factors for Fe-Cr-Al and NiCr in Controlled Industrial Atmospheres," *Materials Science Forum*, 251-254 (1997), 551-558.
9. R. Janakiraman, G. H. Meier and F. S. Pettit, "The Effect of Water Vapor on the Oxidation of Alloys that Developed Alumina Scales for Protection," *Met. Mater. Trans.*, 30A (1999), 2905-2913.
10. K. Onal, M. C. Maris-Sida, G. H. Meier and F. S. Pettit, "Water Vapor Effects on the Cyclic Oxidation Resistance of Alumina-Forming Alloys," *Materials at High Temperature*, 20 (2003), 327-337.
11. E. J. Opila, "Volatility of Common Protective Oxides in High-Temperature Water Vapor: Current Understanding and Unanswered Questions," *Materials Science Forum*, 461-464 (2004), 765-774.
12. B. A. Pint, J. A. Haynes, Y. Zhang, K. L. More and I. G. Wright "The Effect of Water Vapor on the Oxidation Behavior of Ni-Pt-Al Coatings and Alloys," *Surface and Coatings Technology*, 201 (2006), 3852-3856.
13. J. L. Smialek, "Enigmatic Moisture Effects on Al<sub>2</sub>O<sub>3</sub> Scale and TBC Adhesion," *Materials Science Forum*, 595-598 (2008), 191-198.
14. R. Kartono and D. J. Young, "Effectiveness of Pt and Ir in Improving the Resistance of Ni-Al to Thermal Cycling in Air-Steam Mixtures," *Materials and Corrosion*, 59 (2008), 455-462.
15. W. J. Quadackers, J. Žurek, and M. Hänsel, "Effect of water vapor on high temperature oxidation of FeCr alloys," *JOM*, 61(7) (2009), 44-50.
16. V. Déneux, Y. Cadoret, S. Hervier, and D. Monceau, "Effect of Water Vapor on the Spallation of Thermal Barrier Coating Systems During Laboratory Cyclic Oxidation Testing," *Oxidation of Metals*, 73 (2010), 83-93.
17. B. A. Pint and Y. Zhang, "Performance of Al-rich Oxidation Resistant Coatings for Fe-Base Alloys," *Materials and Corrosion*, 62 (2011), 549-560.
18. B. A. Pint, M. P. Brady, Y. Yamamoto, M. L. Santella, P. J. Maziasz and W. J. Matthews, "Evaluation of Alumina-Forming Austenitic Foil for Advanced Recuperators," *Journal of Engineering for Gas Turbines & Power*, 133 (10) (2011), 102302.
19. K. Bouhanek, O. A. Adesanya, F. H. Stott, P. Skeldon, D. G. Lees and G. C. Wood, "High Temperature Oxidation of Thermal Barrier Coating Systems on RR3000 Substrates: Pt Aluminide Bond Coats," *Materials Science Forum*, 369-372 (2001), 615-622.
20. Y. Zhang, J. A. Haynes, B. A. Pint and I. G. Wright, "A Platinum-Enriched  $\gamma+\gamma'$  Two-Phase Bond Coat on Ni-Base Superalloys," *Surface and Coatings Technology*, 200 (2005), 1259-1263.
21. B. Gleeson, "Thermal Barrier Coatings for Aeroengine Applications," *Journal Propulsion & Power*, 22 (2006), 375-383.
22. J. A. Haynes, B. A. Pint, Y. Zhang, K. M. Cooley, L. R. Walker and I. G. Wright, "The Effect of Pt Content on  $\gamma+\gamma'$  Diffusion Coatings," *Surface and Coatings Technology*, 203 (2008), 413-416.
23. B. A. Pint, J. A. Haynes, K. L. More, J. H. Schneibel, Y. Zhang and I. G. Wright, "The Performance of Pt-modified Alumina-Forming Coatings and Model Alloys," *Superalloys 2008*, ed. R. C. Reed, K. A. Green, P. Caron, T. P. Gabb, M. G. Fahrman, E. S. Huron and S. R. Woodard (Warrendale, PA: TMS, 2008), 641-650.
24. B. A. Pint, J. A. Haynes and Y. Zhang, "Effect of Superalloy Substrate and Bond Coating on TBC Lifetime," *Surface and Coatings Technology*, 205 (2010), 1236-1240.
25. J. Stringer, "Coatings in the electricity supply industry: past, present, and opportunities for the future," *Surface and Coatings Technology*, 108-109 (1998), 1-9.
26. Y. Itoh, M. Saitoh and M. Tamura, "Characteristics of MCrAlY Coatings Sprayed by High Velocity Oxygen-Fuel Spraying System," *Journal of Engineering for Gas Turbines & Power*, 122 (2000), 43-49.
27. P. J. Fink, J. L. Miller and D. G. Konitzer, "Rhenium reduction—alloy design using an economically strategic element," *JOM*, 62 (1) (2010), 55-57.
28. W. Y. Lee, Y. Zhang, I. G. Wright, B. A. Pint and P. K. Liaw, "Effects of Sulfur Impurity on the Scale Adhesion Behavior of a Desulfurized Ni-based Superalloy Aluminized by Chemical Vapor Deposition," *Metallurgical Transactions A*, 29 (1998), 833-841.
29. D. K. Gupta and D. S. Duvall, "A Silicon and Hafnium Modified Plasma Sprayed MCrAlY Coating for Single Crystal Superalloys," *Superalloys 1984*, ed. M. Gell, et al. (Warrendale, PA: TMS, 1984), 711-720.
30. K. A. Unocic and B. A. Pint, "Characterization of the Alumina Scale Formed on a Commercial MCrAlYHfSi Coating," *Surface*

and Coatings Technology, 205 (2010), 1178-1182.

31. B. A. Pint, G. W. Garner, T. M. Lowe, J. A. Haynes and Y. Zhang, "Effect of increased water vapor levels on TBC lifetime with Pt-containing bond coatings," *Surface and Coatings Technology*, 206 (2011) 1566-1570.
32. B. A. Pint and J. A. Haynes, "The Effect of Water Vapor Content on TBC Lifetime," *Proceedings of the 8th International Charles Parsons Turbine Conference*, ed. G. M. McColvin, (London, UK: IOM, 2011), G3.3.
33. R. T. Wu, K. Kawagishi, H. Harada and R. C. Reed, "The Retention of Thermal Barrier Coating Systems on Single-Crystal Superalloys: Effects of Substrate Composition," *Acta Materialia*, 56 (2008), 3622-3639.
34. H. M. Tawancy, A. I. Mohamed, N. M. Abbas, R. E. Jones and D. S. Rickerby, "Effect of Superalloy Substrate Composition on the Performance of a Thermal Barrier Coating System," *Journal of Materials Science*, 38 (2003), 3797-3807.
35. U. Schulz, M. Menzebach, C. Leyens, Y. Q. Yang, "Influence of Substrate Material on Oxidation Behavior and Cyclic Lifetime of EB-PVD TBC Systems," *Surface and Coatings Technology*, 146-147 (2001), 117-123.
36. P. Deb, D. H. Boone and T. F. Manley, "Surface Instability of Platinum Modified Aluminide Coatings During 1100°C Cyclic Testing," *Journal of Vacuum Science & Technology A*, 5 (1987), 3366-3372.
37. V. K. Tolpygo and D. R. Clarke, "Rumpling of CVD (Ni,Pt)Al diffusion coatings under intermediate temperature cycling," *Surface and Coatings Technology*, 203 (2009), 3278-3285.
38. A. M. Karlsson, T. Xu and A. G. Evans, "The effect of the thermal barrier coating on the displacement instability in thermal barrier systems," *Acta Materialia*, 50 (2002) 1211-1218.
39. N. M. Yanar, F.S. Pettit and G.H. Meier, "Failure Characteristics during Cyclic Oxidation of Yttria Stabilized Zirconia Thermal Barrier Coatings Deposited via Electron Beam Physical Vapor Deposition on Platinum Aluminide and on NiCoCrAlY Bond Coats with Processing Modifications for Improved Performances," *Metallurgical and Materials Transactions A*, 37 (2006), 1563-1580.
40. H. E. Evans, "Oxidation failure of TBC systems: An assessment of mechanisms," *Surface and Coatings Technology*, 206 (2011), 1512-1521.
41. I. T. Spitsberg, D. R. Mumm and A. G. Evans, "On the Failure Mechanisms of Thermal Barrier Coatings with Diffusion Aluminide Bond Coatings," *Materials Science & Engineering*, A394 (2005), 176-191.
42. B. A. Pint, S. A. Speakman, C. J. Rawn and Y. Zhang, "Deformation and Phase Transformations During Cyclic Oxidation of Ni-Al and Ni-Pt-Al," *JOM*, 58(1) (2006), 47-52.
43. H. E. Evans and R. C. Lobb, "Conditions for the Initiation of Oxide-Scale Cracking and Spallation," *Corrosion Science*, 24 (1984), 209-222.
44. J. A. Haynes, B. A. Pint, K. L. More, Y. Zhang, and I. G. Wright, "Influence of Sulfur, Platinum and Hafnium on the Oxidation Behavior of CVD NiAl Bond Coatings," *Oxidation of Metals* 58 (2002), 513-544.
45. B. A. Pint, K. L. More and I. G. Wright, "The Effect of Quaternary Additions on the Oxidation Behavior of Hf-Doped NiAl," *Oxidation of Metals*, 59 (2003), 257-283.
46. V. K. Tolpygo, K. S. Murphy and D. R. Clarke, "Effect of Hf, Y, C in the Underlying Superalloy on the Rumpling of Diffusion Aluminide Coatings," *Acta Materialia*, 56 (2008), 489-499.
47. B. A. Pint and K. L. More, "Characterization of Alumina Interfaces in TBC Systems," *Journal of Materials Science*, 44 (2009), 1676-86.
48. J. L. Smialek, "Martensite in NiAl Oxidation Resistant Coatings," *Metallurgical Transactions*, 2A (1971), 913-915.
49. Y. Zhang, J. A. Haynes, B. A. Pint, I. G. Wright, and W. Y. Lee, "Martensitic Transformation in CVD NiAl and (Ni,Pt)Al Bond Coatings," *Surface and Coatings Technology*, 163-164 (2003), 19-24.
50. J. Doychak and M. Rühle, "TEM Studies of Oxidized NiAl and Ni<sub>3</sub>Al Cross Sections," *Oxidation of Metals*, 31 (1989), 431-452.
51. B. A. Pint, A. J. Garratt-Reed and L. W. Hobbs, "Analytical Electron Microscopy Study of the Breakdown of  $\alpha$ -Al<sub>2</sub>O<sub>3</sub> Scales Formed on Oxide Dispersion Strengthened Alloys," *Oxid. Met.*, 56 (2001), 119-145
52. J. A. Haynes, B. A. Pint, W. D. Porter and I. G. Wright, "Comparison of Thermal Expansion and Oxidation Behavior of Various High-Temperature Coating Materials and Superalloys," *Mater. High Temp.*, 21 (2004), 87-94.
53. B. A. Pint, "The Future of Alumina-Forming Alloys: Challenges and Applications for Power Generation," *Material Science Forum*, 696 (2011), 57-62.
54. B. A. Pint, W. D. Porter and I. G. Wright, "The Effect of Thermal Expansion on Spallation Behavior of Fe-Base Alumina-Forming Alloys," *Materials Science Forum*, 595-598 (2008), 1083-1092.
55. K. Harris and J. B. Wahl, "Improved Single Crystal Superalloys. CMSX-4@(SLS)[La+Y] and CMSX-486@," *Superalloys 2004*, ed. K. A. Green, T. M. Pollock, H. Harada, T. E. Howson, R. C. Reed, J. Schirra and S. Walston (Warrendale, PA: TMS, 2004), 45-52.
56. F. S. Pettit, E. H. Randklev and E. J. Felten, "Formation of NiAl<sub>2</sub>O<sub>4</sub> by Solid State Reaction," *Journal of the American Ceramic Society*, 49 (1966), 199-203.
57. D. J. Young, D. Naumenko, L. Niewolak, E. Wessel, L. Singheiser and W. J. Quadakkers, "Oxidation kinetics of Y-doped FeCrAl-alloys in low and high pO<sub>2</sub> gases," *Materials and Corrosion*, 61 (2010) 838-844.
58. K. A. Unocic, E. K. Essuman, S. Dryepondt, and B. A. Pint, "Effect of Environment on the Scale Formed on ODS FeCrAl at 1050°-1100°C," *Materials at High Temperature*, in press (2012).
59. B. A. Pint, M. A. Bestor and J. A. Haynes "Cyclic Oxidation Behavior of HVOF Bond Coatings Deposited on La- and Y-doped Superalloys," *Surface & Coatings Technology*, 206 (2011), 1600-1604.
60. K. A. Unocic, C. M. Parish and B. A. Pint, "Characterization of the Alumina Scale formed on Coated & Uncoated Doped Superalloys," *Surface Coatings Technol.* 206 (2011), 1522-1528.